Analysis of Cavitation-Induced Pressure Loads on Compliant Polymer Coatings

by

Ajay Panwar

A Thesis Presented in Partial Fulfillment
of the Requirement for the Degree
Master of Science

Approved April 2015 by the
Graduate Supervisory Committee:

Jay Oswald, Chair
Kevin Dooley
Kangping Chen

ARIZONA STATE UNIVERSITY

May 2015

ABSTRACT

Cavitation erosion is a significant cause of wear in marine components, such as impellers, propellers or rudders. While the erosion process has been widely studied on metals, the effect of cavitation on polymers is not well-understood. The stress response in metals differs greatly from that of polymers, e.g. rate and temperature effects are far more important, thus damage and wear mechanisms of polymers under cavitating flows are significantly different. In this work, heat-driven failure caused by viscous dissipation and void nucleation resulting from tensile stresses arising from stress wave reflections are investigated as two possible material failure mechanisms.

As a first step in developing a fundamental understanding of the cavitation erosion process on polymer surfaces, simulations are performed of the collapse of individual bubbles against a compliant surface e.g. metallic substrates with polyurea coatings. The surface response of collapse-driven impact loads is represented by a idealized, time-dependent, Gaussian pressure distribution on the surface. A two-dimensional distribution of load radii and durations is considered corresponding to characteristic of cavitating flows accelerated erosion experiments. Finite element simulations are performed to fit a response curve that relates the loading parameters to the energy dissipated in the coating and integrated with collapse statistics to generate an expected heat input into the coating.

The impulsive pressure, which is generated due to bubble collapse, impacts the material and generates intense shock waves. The stress waves within the material reflects by interaction with the substrate. A transient region of high tensile stress is produced by the interaction of these waves. Simulations suggests that maximum hydrostatic tension which cause failure of polyurea layer is observed in thick coating. Also, the dissipated viscous energy and corresponding temperature rise in a polyurea is calculated, and it is concluded that temperature has influence on deformation.

To my Beloved Parents

The reason of what I became today

Thanks for your great support and continuous care!!

ACKNOWLEDGEMENTS

I would like to express my sincere gratitude and thanks to my advisor, Professor Dr. Jay Oswald, for his continuous guidance and encouragement throughout my research work. His intellectual support helped me organize my research endeavors into a thesis. I also wish to extend my gratitude to my thesis committee, Dr. Kevin Dooley and Dr Kangping Chen, for their guidance and valuable suggestions.

I am also thankful to Xiao Liao (PhD student) for his valuable assistance in this project and for giving me attention and time. I also wish to extend my gratitude to the whole computational mechanics lab group. It would not have been possible to complete the project without the kind support and help of many individuals from the group. Words are inadequate in offering my thanks to everyone for their encouragement and cooperation in carrying out the project work.

Finally, yet importantly, I would like to express my heartfelt thanks to my beloved parents for their blessings. And appreciation also goes to my colleagues in developing the project and people who have willingly helped me out with their abilities.

TABLE OF CONTENTS

CHAPTER Page

LIST OF TABLES

LIST OF FIGURES

Figure Page

Chapter 1

INTRODUCTION

Cavitation is the process of vapor cavity formation in liquids (Brennen (2013); Franc and Michel (2006)), that occurs when the liquid is subjected to a rapid decrease in pressure. Vapor cavities break up in to clouds of bubbles that then collapse when they are advected into high pressure regions. When bubbles collapse in the vicinity of a surface (e.g. near an impeller as shown in Figure 1.1), the collapse is asymmetric and produces a strong jet that impacts the surface with extreme pressure. The combined effect of many of such impacts causes erosive wear on the surface that eventually leads to mass loss.

When cavitation bubbles collapse, they generate very high local pressure near metal surfaces and cause cyclic stress through repeated implosion (Choi *et al.* (2014); Zhang *et al.* (1993); Thiruvengadam (1974)). Cavitation erosion is fairly well understood for metal surfaces, however, there is recent interest in developing polymer coatings to protect marine surfaces against cavitation erosion. The effects of cavitation erosion on polymers is far less well understood, and thus this research aims to develop a basic understanding of the effect of bubble collapse on polymers.

1.1 Modeling of Cavitation Erosion

Since cavitation flows generate a wide distribution of different bubble sizes and collapse pressures, it is important to determine a measure of the intensity of the cavitation field. The cavitation intensity depends on the size of the bubble collapse. The low-pressure bubble in a liquid begins to collapse due to the higher pressure of the surrounding medium. The bubble eventually collapses to a minute fraction of

Figure 1.1: Cavitation Erosion in Single Vane Impeller Reproduced from Thamsen *et al.* (2008)

its original size, as the bubble collapses, the pressure and temperature of the vapor within increases. At this point the gas within dissipates into the surrounding liquid via a rather violent mechanism which releases a significant amount of energy. This violent behavior of energy makes huge impact on the surface and the intensity of it, is linked with the size of the bubble collapse.

When the impact load intensity exceeds the threshold cavitation intensity, cavitation leads to erosion in the polyurea. That is, material is removed due to a high impact load when the bubble collapses and causes formation of pits on the order of several tens of micrometers that lead to material failure (Pereira *et al.* (1998); March (1987); Soyama *et al.* (1998); Ahmed *et al.* (1991)).

Pitting tests have been used to estimate the distribution of impulsive loads and and their characteristic length scales in a cavitating flow. These are short duration tests that are dependent on the impact load, where metals record pits or permanent deformations from recurring cavitation events. Metal pits were measured using a profilometer (Carnelli *et al.* (2012)). This technique, which is relatively effective for

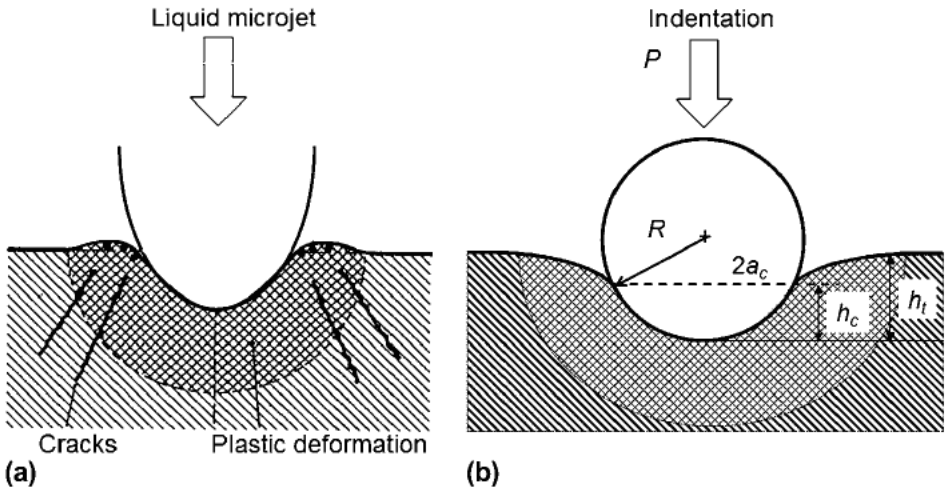

Figure 1.2: Represents the Similarities in Deformation Under (a) Liquid impact (b) Indentation Testing Reproduced from Carnelli *et al.* (2012)

determining cavitation shape, assumes that the material itself is a sensor capable of detecting the impact loads through permanent deformations of the surfaces generated by individual impact events. After taking the mechanical parameters of the test material by spherical nanoindentation technique, pitting tests are performed at different pressures, and the geometric characteristics of the pits are then measured. By analyzing the tests, the final spectra of the impact pressures and loads responsible for material erosion were obtained, and the aggressiveness of the cavitating flow was quantified. As such, the spherical shape distortion imposed by nanoindentation and the hydrodynamics of cavitation erosion is shown in Figure 1.2.

Nanoindentation can not be performed on the polymers. Since, polymers are much more compliant, so shape is a significant factor. Different methods are therefore needed for polymers. This is further apparent given that metals show low strain rates under impacts, whereas polymers display larger strain rate effects. Hence, the test material must be well enough understood to determine what types of impact cause

pits. Moreover, it is not yet clear if there is a one-to-one relationship between loading parameters and pit geometry (Carnelli *et al.* (2012)).

Franc *et al.* (2011) measured the impact loads generated by cavitation bubble collapse by mounting a conventional pressure sensor in a region on a surface where maximum damage was observed. These pressure transducers are capable of undergoing severe cavitation erosion and can capture short duration loads with very small time resolution of 2µs. To remove the dependence of signal height on area, these pressure transducers are much larger than the size of the impacts. Pressure pulse magnitudes were measured at different velocities, and it was found that they follow an exponential law that depends on the reference peak rate and reference load as shown in Eq. 1.1.

$$\dot{N} = \dot{N}_0 e^{-} \frac{F}{F_0} \tag{1.1}$$

These measured impact load results are compared with the pitting tests, from which it is concluded that uncertainty remains on the measured impact load values. The two dimensional histogram technique was suggested (Franc *et al.* (2011)) to generate a more complete description of the cavitation intensity.

The function for one dimensional density distribution where bubble radius and impact pressure are varying individually is represented in the following equations (Kim *et al.* (2014)):

$$N^* = \int_0^\infty P(r)dr = \int_O^\infty P(p)dp \tag{1.2}$$

where P(r) and P(p) is the probability density of impacts shown below with parameters, bubble radius (r) and maximum pressure magnitude (p) with N^* (impacts/cm^2/sec) hydrodynamics impacts,

$$P(r) = \frac{N^*}{R^*} e^{-r/R^*} \tag{1.3}$$

$$P(p) = \frac{N^*}{P^*} e^{-p/P^*} \tag{1.4}$$

P^*, R^* are reference bubble radius and impact pressure magnitude to the slope of exponential law

The function for two dimensional density distribution considering bubble radius and impact pressure as a independent variables is shown below,

$$P(r, P) = P(r)P(p) \tag{1.5}$$

This, results in the two dimensional number probability distribution,

$$P(r, P) = \frac{N^*}{P^* R^*} e^{-r/R^*} e^{-p/P*} \tag{1.6}$$

Cavitation erosion has also been modeled by a empirical expression Choi *et al.* (2012) in terms of the mean depth of erosion versus time. Normalized cavitation erosion depth is represented as $\bar{h} = 1 - e^{-t^2} + e^{-1}\bar{t}^{1.2}$ where t is normalized time and h is the mean erosion depth. Several erosion progression tests with varying erosion field intensities were obtained using modified ASTM-G32 (ast (2010)) and DYNAFLOW's (Choi *et al.* (2012)) cavitating jet techniques. Different test parameters were obtained, which resulted in the above co-relation.

1.2 Characteristics of Cavitation on Metals

So far, several methods have been developed for predicting the response of materials subjected to cavitation. Choi *et al.* (2012) explained a mathematical model to represent cavitation erosion which is a function of cavitation mean depth and time of

cavitating jets. This experiment was carried out using ultrasonic cavitation erosion testing (ASTM G32) and cavitating testing jets (ASTM G134). These tests were performed when bubble collapse occurred on contact with the material, i.e. there was no use of any wear protecting layer.

Cavitation erosion occurs, for example, on propellers due to large hydrostatic stresses. It is not necessary that the material respond just after its contact with a high pressure impact load. Metals, in general, show some resistance and undergo changes before erosion begins. The stages of cavitation erosion are explained below.

Incubation Stage: The initial phase begins with the contact of cavitating jets with the material, and the surface becomes more stress resistant. There are variations in this process depending on the material, but in general, some microscopic change in the material occurs and the surface gets deformed but without any material loss. The stage is also accompanied with the hardening of the surface which may also leads to permanent deformation during this phase.

Acceleration Stage: Following the incubation period, the erosion rate increases until it attains maximum erosion, resulting in large material loss followed by fractures, as shown in Figure 1.3. This period includes the interaction of the cavitating jets with up to several inner layers of the material.

Attenuation Stage: The erosion process decelerates as the roughness of the fragmented surface leads to bubble cushioning.

Terminal stage: Local equilibrium is reached between the response of the material and the erosive power of the cavitation field. That is, erosion process enters the steady-state period, where the rate of weight loss reaches a constant value.

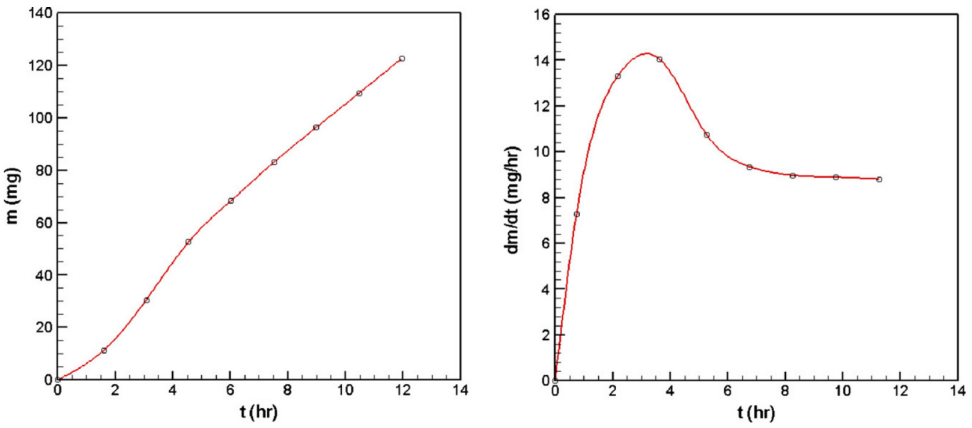

Figure 1.3: Weight Loss Erosion S-curve and Erosion Rate Curve v/s Time Reproduced from Choi *et al.* (2012)

1.3 Characteristics of Cavitation on Polymers

The cavitation erosion in polymers is significantly different than the effect of cavitation erosion on metals. The stress response in polymers has a much higher sensitivity to temperature than in metals. As a result, the heat generated from the dissipation of cavitation impact loads, is expected to play a much more prominent role in the durability of the material. At low temperatures, polymers have higher strength, but also may experience brittle fracture, while at high loads, polymers become much more viscous and rubbery, yet lose strength. Polymers generally show the behavior both of liquid and solids, in that they exhibit viscous flow, yet due to cross-linking and entanglement networks, eventually regain their original shape once a load is removed.

The glass transition temperature T_g is an important characteristic of polymers. When the temperature of the polymer rises above T_g, it becomes more rubber-like and when temperature drops below T_g, the polymer is increasingly brittle. Thus, values of T_g well below room temperature define elastomers (such as polyurea) and those above room temperature define structural, rigid polymers for example, polycarbonate.

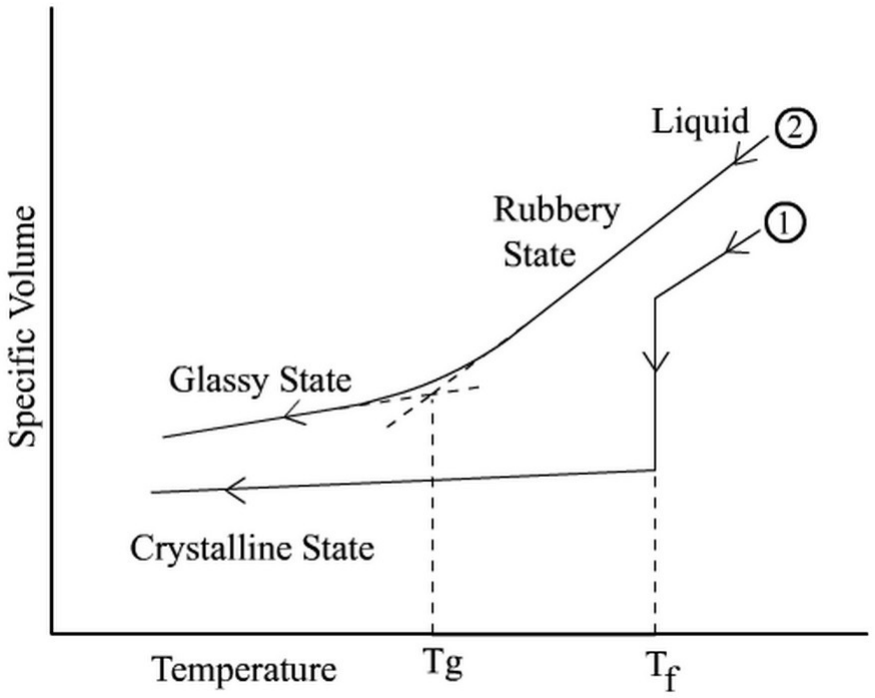

Figure 1.4: Characteristics of Polymers Reproduced from Foreman *et al.* (1994)

For the characterization of the liquid-glass transition phenomenon T_g, note that there is no step change in volume when cooling an amorphous material from the liquid state, although the rate of decrease may vary. There is, however, a step change when a crystalline material approaches its freezing point, T_f, as shown in Figure 1.4

1.4 Objectives and Scope

Polyurea is a material commonly used for protection from mechanical wear. It is an elastomer obtained by the reaction of an isocyanate component with synthetic resin. It is extensively used in the coating industry, for example polyurea coatings in steel tanks protects from corrosion. Polyurea is also commonly used in truck bed liners as shown in Figure 1.5 and protects utility trucks from harsh duty environments.

The main objective of this research is to determine the rate of viscous energy

Figure 1.5: Polyurea Coated Truck Bed Liners

dissipated on a polymer surface when exposed to a cavitating flow. This research also tries to understand how the geometry of the coating, example thickness is related to its durability.

Chapter 2

MATERIAL MODEL OF POLYMERS

The behaviour of polymers is time dependent due to their molecular structure. Polymers behave differently than other time dependent materials like metals that experience fatigue and corrosion. This chapter explains the material model for polymers.

2.1 Linear Viscoelasticity

Viscoelasticity is the property of polymers which exhibit viscous and elastic characteristics while undergoing deformation when external force is applied (Brinson and Brinson (2007)). The linearity of any model can only be accessed if the material is independent of stress despite of loading type. Let's first discuss the importance of relaxation and then creep in viscoelasticity. In relaxation, the material under test is kept consistently strained over a period of time and stress is measured. After the application of stress, material relaxes due to the effect of viscousity in material over time. Thus, if the stress is a function of time and strain is kept constant then modulus in viscoelastic material will vary with time. Hence, modulus is inherently a function of time.

Figure 2.1 shows stress in the relaxation test,

$$G(t) = \frac{\sigma(t)}{\epsilon_0} = \text{Relaxation modulus} \tag{2.1}$$

And modulus for $t = 0$ and at $t = \infty$ is defined as

$$G(t = 0) = \frac{\sigma(t = 0)}{\epsilon_0} = G_0 = \text{Initial modulus} \tag{2.2}$$

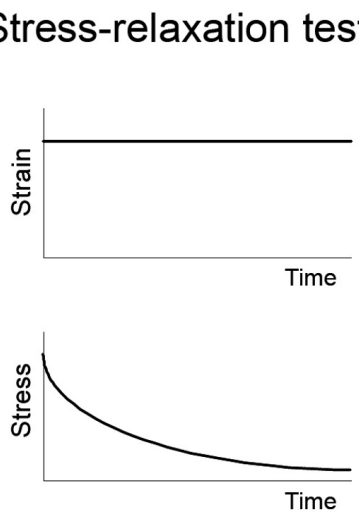

Figure 2.1: Stress Relaxation Test Illustrating Strain Input and Stress Output Reproduced from Murata (2012)

$$G(t=\infty) = \frac{\sigma(t=\infty)}{\epsilon_0} = G_\infty = \text{Equilibrium modulus} \tag{2.3}$$

The creep test is defined as the case where the strain in material under the influence of constant stress increases with time. Rate of deformation depends upon some material properties such as exposure time, applied load etc.

Figure 2.2 below represents the strain response in the creep test

$$D(t) = \frac{\epsilon(t)}{\sigma_0} = \text{Creep compliance} \tag{2.4}$$

Thus polymers have characteristics of both solids and fluids. The linearity of the model is defined by when the creep compliance is independent of stress. The relaxation modulus is independent of strain, this will be discussed later. The basic Maxwell model composite of spring and dashpot as shown in Figure 2.3, and the relation between stress and strain, can be developed by using constitutive equations

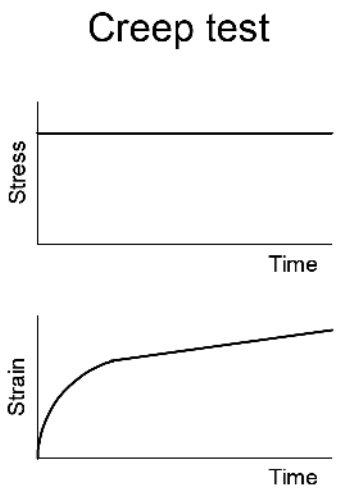

Figure 2.2: Creep Test Illustrating Stress Input and Resulting Strain Reproduced from Murata (2012)

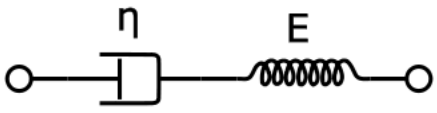

Figure 2.3: Maxwell Model

of the elements. By using kinematic and equilibrium conditions in the system, the stress of the Maxwell element will be the same in both the spring and dashpot and the total strain will be equal to the sum of the spring and dashpot strains.

$$\sigma = \sigma_s = \sigma_d \tag{2.5}$$

$$\epsilon = \epsilon_s + \epsilon_d \tag{2.6}$$

constitutive equations of spring and dashpot are,

$$\sigma_s = E\epsilon_s = \sigma \tag{2.7}$$

$$\sigma_d = \mu \frac{d\epsilon_d}{dt} = \mu \dot{\epsilon_d} = \sigma \tag{2.8}$$

Differentiating Eq. 2.6 and substituting strain rates into constitutive equations of spring and dashpot yields,

$$\sigma + \frac{\mu}{E}\dot{\sigma} = \mu\dot{\epsilon} \tag{2.9}$$

The inverse of the coefficient of stress is the relaxation time, $\tau = \mu/E$, following that, by using the step input function in strain we get,

$$\epsilon(t) = \epsilon_0 \mathrm{H}(t) \tag{2.10}$$

where $\mathrm{H}(\cdot)$ is Heaviside or a unit step function whose significance is defined as it is identically zero for all negative values and equals to one when its argument is positive, we will get the stress output.

Since in stress relaxation, $\dot{\epsilon} = 0$, Eq. 2.9 becomes,

$$\frac{d\sigma}{dt} = -\frac{1}{\tau}\sigma \tag{2.11}$$

Separating variables and integrating Eq. 2.11,

$$\int_{\sigma_0}^{\sigma} \frac{d\sigma}{\sigma} = -\frac{1}{\tau}\int_0^t dt \tag{2.12}$$

$$\log\sigma - \log\sigma_0 = -\frac{t}{\tau} \tag{2.13}$$

$$\sigma(t) = \sigma_0 e^{-t/\tau} \tag{2.14}$$

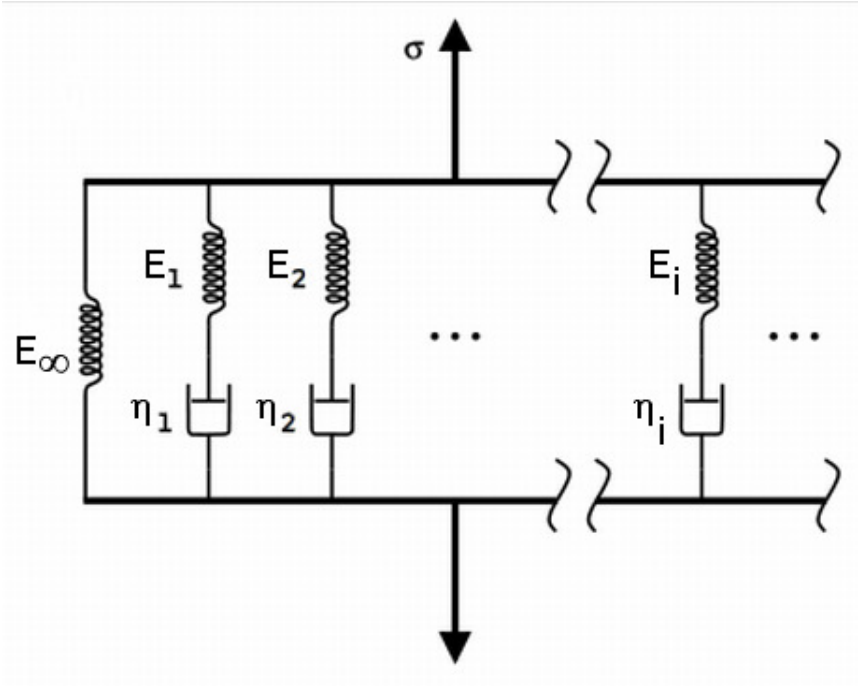

Figure 2.4: Generalized Maxwell Model

This gives the physical significance of relaxation time, which is stated as the time needed for the stress to fall to $1/e$ of its initial value. Hence, the relaxation modulus $G(t)$ can be obtained directly from this relation as,

$$G(t) = \frac{\sigma(t)}{\epsilon_0} = \frac{\sigma_0}{\epsilon_0} e^{-t/\tau} \tag{2.15}$$

$$G(t) = G_0 e^{-t/\tau} \tag{2.16}$$

Now, let's derive the equation for the Generalized Maxwell Model, where Maxwell elements are connected in parallel as shown in Figure 2.4, by considering the stress relaxation case where constant strain history is applied. The kinematic constraint that gives strain will be constant in each element and thus the global stress will be equal to the sum of individual stresses $\sigma(t) = \sigma_1(t) + \sigma_2(t) + ... + \sigma_n(t)$.

$$\sigma(t) = \epsilon_0(E_1 e^{-t/\tau_1} + E_2 e^{-t/\tau_2} + \cdots + E_i e^{-t/\tau_i}) \tag{2.17}$$

By solving above equation gives,

$$\sigma(t) = \epsilon_0 \sum_{i=1}^{n} E_i e^{-t/\tau_i} \tag{2.18}$$

From the above equation, the relaxation modulus of the Generalized Maxwell Model is given by,

$$G(t) = \sum_{i=1}^{n} G_i e^{-t/\tau_i} \tag{2.19}$$

This series is known as the Prony series.

By including a free spring in the generalized model, we can represent thermoset polymers, giving us a long term modulus, i.e. G_∞, when the material is totally relaxed. This model is also known as the Wiechert model. The solution of the stress and relaxation modulus will be,

$$\sigma(t) = \epsilon_0 \left(\sum_{i=1}^{n} G_i e^{-t/\tau_i} + G_\infty \right) \tag{2.20}$$

$$G(t) = \sum_{i=1}^{n} G_i e^{-t/\tau_i} + G_\infty \tag{2.21}$$

where G_∞ is a long term shear moduli and $G_i/G_\infty = p_i$, then the equation can be rewritten as,

$$G(t) = G_\infty \left(1 + \sum_{i=1}^{n} p_i e^{-t/\tau_i} \right) \tag{2.22}$$

Now, considered variable stress input in order to find strain output. If we consider the variable stress inputs as a series of steps at variable time, this will give us,

$$\sigma(t) = \sigma_0 H(t) + (\sigma_1 - \sigma_0)H(t - t_1) + \cdots + (\sigma_n - \sigma_{n-1})H(t - t_n) \tag{2.23}$$

Creep compliance is discussed earlier, thus on the basis of that creep response for single step input can be written as,

$$\epsilon(t) = \sigma_1 D(t - t_1) \quad \text{for} \quad \sigma(t) = \sigma_1 H(t - t_1) \tag{2.24}$$

above, the strain output for a varying stress input can be illustrated as the sum of the output of every individual step, which can be represented as,

$$\epsilon(t) = \sigma_0 D(t)H(t) + (\sigma_1 - \sigma_0)D(t - t_1)H(t - t_1) + (\sigma_2 - \sigma_1)D(t - t_2)H(t - t_2) + \\ \ldots + (\sigma_n - \sigma_{n-1})D(t - t_n)H(t - t_n)$$

$$\epsilon(t) = \sigma_0 D(t)H(t) + \sum(\sigma_n - \sigma_{n-1})D(t - t_n)H(t - t_n) \tag{2.25}$$

The time increment for each step is, $\Delta\tau$, and considering $\Delta\tau$ approaches zero, we will end up with,

$$\epsilon(t) = \sigma_0 D(t)H(t) + \int_{0^+}^{t} D(t - \tau)\frac{d\sigma(\tau)}{d\tau}d\tau \tag{2.26}$$

We can rewrite the above equation as,

$$\epsilon(t) = \int_{0}^{t} D(t - \tau)\frac{d\sigma(\tau)}{d\tau}d\tau \tag{2.27}$$

Stress is expressed in terms of the Heaviside function as, $\sigma(t) = \sigma(t)H(t)$ and the lower limit t = 0^+ indicates the jump discontinuity in the stress. By using this in Eq.2.26 and differentiating it, we get,

$$\epsilon(t) = \int_{0^+}^{t} D(t-\tau)\left(\frac{d[\sigma(\tau)]}{d\tau}H(\tau) + \sigma(\tau)\delta(\tau)\right)d\tau \tag{2.28}$$

Due to the shifting property of the Dirac delta function, the equation can be reduced to,

$$\epsilon(t) = \int_{0^+}^{t} D(t-\tau)\frac{[d\sigma(\tau)]}{d\tau}d\tau \tag{2.29}$$

Similarly, we can get the stress output for the variable strain input, i.e.,

$$\sigma(t) = \int_{0}^{t} G(t-\tau)\frac{d\epsilon(\tau)}{d\tau}d\tau \tag{2.30}$$

This is the basic hereditary integral formulation for linear isotropic viscoelasticity. Furthermore, temperature could come into play that could lead to residual stress and creating changes to the molecular structure of the polymer.

Figure 2.5 represents the similarity in stress output between theoretical, where strain history is considered to get the theoretical stress, whereas in numerical simulations, where stress is obtained recursively.

This stress routine gives us proof of our working viscoelastic model. This model will now be further extended to account for temperature dependence.

2.2 Temperature and Pressure Dependence

The temperature model can be explained by Williams-Landel-Ferry theory (Amirkhizi *et al.* (2006)) on time-temperature and pressure sensitivity with the inclusion of a thermal mechanism of polyurea.

The effects of temperature on material response is stated by the following points:
1. At high temperature, short time relaxation of the material appears which changes the response of relaxation, and actuated frequently and the material gets relaxed

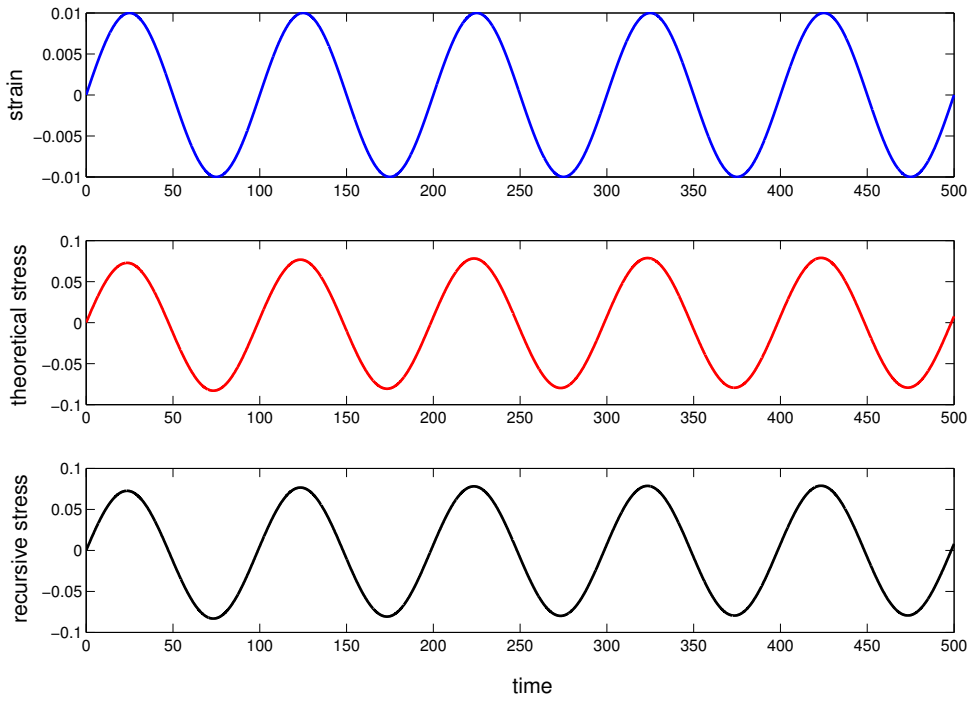

Figure 2.5: Stress Routine

more easily

2. Long time change in moduli in terms of absolute temperature

The equation below represents these two effects,

$$G(t,T) = \frac{T}{T_0} G_0 \left(\frac{t}{a(T)} \right) \tag{2.31}$$

Here "a" is a shift function, which expresses in terms of current temperature, T_0, and the glass transition temperature, T_g. The relaxation function derived above using the Prony series is,

$$G_0(t) = G_\infty \left(1 + \sum_{i=1}^{n} p_i e^{-t/q_i} \right) \tag{2.32}$$

where p_i is the relative modulus in terms of i and q_i is dissipation time. Now, the

deviatoric stress equation and the relaxation modulus in terms of reduced time can be expressed as,

$$\sigma'(t) = \int_0^t 2G(t,\tau)D'(\tau)d\tau \tag{2.33}$$

$$G(t,T) = \frac{T(\tau)}{T_0}G_0(\xi(t) - \xi(\tau)) \tag{2.34}$$

The deformation of the material is influenced by temperature and can be expressed as a new reduced time function $\xi(t)$ in terms of temperature and pressure.

$$\xi(t) = \int_0^t \frac{d\tau}{a(T(\tau)p(\tau))} \tag{2.35}$$

where the temperate changes during deformation is expressed in terms of reduced time function with new time scale,

$$\xi(t) = \int_0^t \frac{d\tau}{a(T(\tau))} \tag{2.36}$$

$a(\tau)$ is a time-temperature shift function with dependence on current temperature and the glass transition temperature, T_g, of the material. Knauss (2004) on the other hand obtained the value of polyurea and arrived upon the time-temperature shift function for polyurea,

$$a(T) = 10^{A(T-T_0)/(B+(T-T_0))} \tag{2.37}$$

Since viscoelastic properties of polymers are pressure dependent, thus to incorporate the pressure term in the model, it can be set as,

$$a(T,P) = a(T - C_{tp}P) \tag{2.38}$$

where, C_{tp} is time pressure coefficient.

Material internal relaxation terms are calculated by constructing a discrete set of internal variables. Dissipated energy can be calculated and stored in terms of elastic energy of their last step after all the iterations. By using n internal variables and linear force flux equations we get the relaxation modulus of Prony series.

The heat source in material come from dissipated mechanical energy, where the local change in temperate due to deformation is,

$$\frac{\partial T}{\partial t} = \frac{1}{C_v}\frac{\partial W_d}{\partial t} \tag{2.39}$$

where C_v is the heat capacity constant per unit volume and W_d is the dissipated work per unit original volume. The amount of dissipated energy associated with the i^{th} internal variable is represented as,

Table 2.1: Material Parameters Used in the Numerical Model

T_{ref}:	273 (K)	B:	107.53 (K)
A:	-10	n:	4
C_v:	1.977×10^{-3} (J mm^{-3}K^{-1})	CTE:	2×10^{-4} (K^{-1})
m:	-0.015 (GPa K^{-1})	C_{tp}:	7.2 (K GPa^{-1})
κ_{ref}:	4.948 (GPa)	G_∞:	0.0224 (GPa)

$$\frac{\partial W_d^i}{\partial t} = \frac{1}{\eta^i}(F^i)^2 \tag{2.40}$$

here, n^i is viscosity and F is the force linked with the ith internal variable,

Thus, in deformation, dissipated energy by viscosity and force due to internal variable is represented by,

$$\frac{\partial W_d}{\partial t} = 2G_\infty\frac{T(t)}{T_0}\sum_{i=1}^{n}\frac{p_i}{q_i}\epsilon_d^i(t) : \epsilon_d^i(t) \tag{2.41}$$

Equation 4.2 represents the dissipated energy having i^{th} internal variables and relates to the relaxation modulus in Eq 2.32.

Material parameters used in the numerical model are listed in Table 2.1.

2.3 Efforts to Characterize Polyurea

Polyurea is a cross-linked amorphous isocyanate monomer or prepolymer and polyamine curative. To be classified as a polyurea, the compound must contain at least 80% polyamine (Tekalur *et al.* (2008)). It is usually applied using a spray coating system in a 1:1 mix ratio.

Iscocynate in polyurea can be aromatic and aliphatic system (Tekalur *et al.* (2008)). Aromatic polyureas are based on an aromatic diisocyanate. Their performance level is excellent, though these are not light-stable but they do not degrade their physical properties when exposed to light. Whereas aliphatic polyureas based on an aliphatic diisocyanate are light-stable, which means they do not change colour when exposed to light (artificial or sun) therefore they are more difficult to process. Polyurea has excellent bonding with carefully prepared substrates, for example aluminium substrates, but acceptable bond strength can be achieved on slightly humid surfaces. Polyurea is extremely resistant to thermal shock and blast effects and also has good chemical resistance and is self-extinguishing when the flame is removed from the surface. The tensile strength of polyurea is 20-30 MPa, 350 % elongation and 87.5kN/m tear strength (Tekalur *et al.* (2008)).

2.3.1 Split-Hopkinson Bar Experiment

To verify the model that we discussed in previous section, tests on polyurea were conducted using split-Hopkinson bar experiments (SPHB) by Nemat-Nasser (Nemat-Nasser *et al.* (1991); Amirkhizi *et al.* (2006)). All tests were performed at an effective

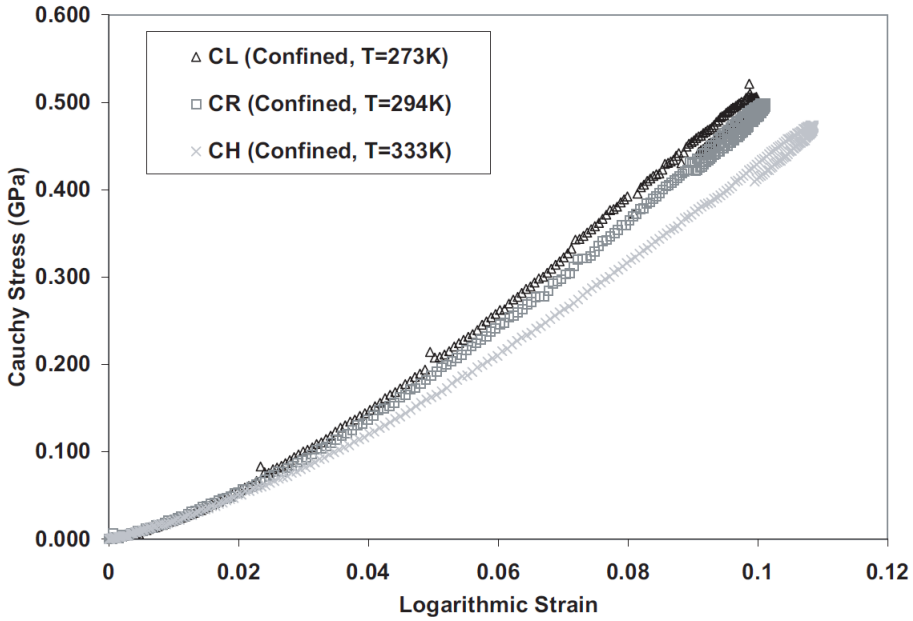

Figure 2.6: Confined Split-Hopkinson Bar Experiment Stress-Strain Results Reproduced from Amirkhizi *et al.* (2006)

engineering strain rate of 3000 ± 400 s^{-1}. There were two types of loading on SPHB specimen carried out: confined and unconfined loading.

In the unconfined loading, deformation can take place in multi-direction where as in confined loading the deformation is only possible in axial direction. Under a unconfined test, the sample diameter was substantially smaller than that of the bars to accommodate the large radial deformation that occurred during the tests. Strain in the transmitted bar in an unconfined test was as low as 10^{-4}.

In confined tests, the Cauchy stress and nominal stress were directly equal due to confinement. But in unconfined tests, the diameter of the sample changes. Thus, the Cauchy stress must be evaluated. Cauchy stress and diameter were calculated assuming isochoric deformation since low pressure was observed in the unconfined tests. Resulting confined and unconfined stress-strain curves are shown in Figures 2.6

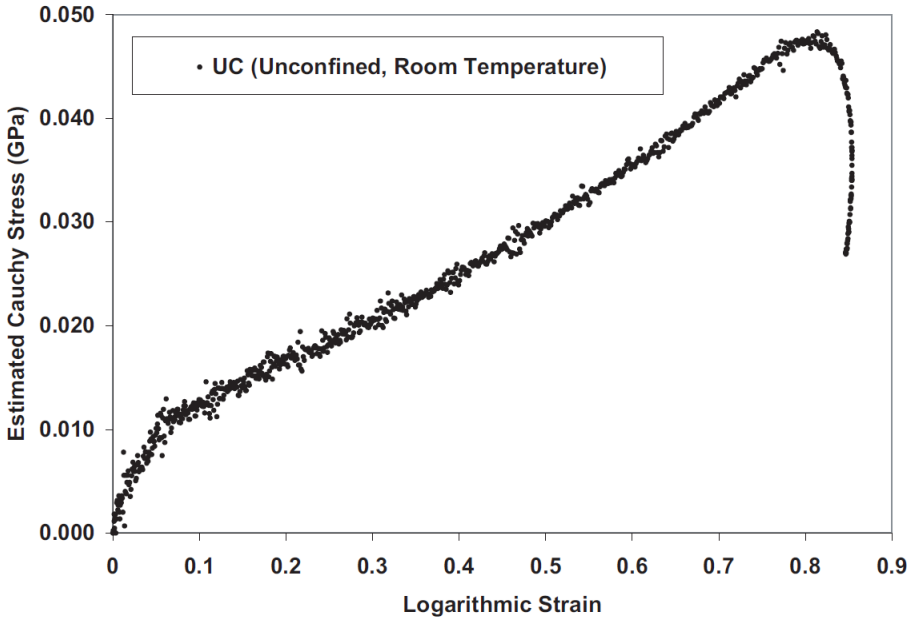

Figure 2.7: Unconfined Split-Hopkinson Bar Experiment Stress-Strain Results Reproduced from Amirkhizi *et al.* (2006)

and 2.7.

Unloading in confined tests follows the same stress-strain curve as that of loading. However, stress was released much faster than the accumulated strain in unconfined tests. The strain was not permanent in any tests and strain occurred at a low rate and was limited to 1% - 2%.

2.3.2 Dynamics Mechanical Analysis

The Dynamic mechanical analysis (DMA) were carried to check the dependency of viscoelastic properties of polyurea on temperature and frequency. DMA of the samples was conducted by Boyce et al. (Yi *et al.* (2006); Qiao *et al.* (2011)). Samples from both end were constrained from rotation and sliding by clamping plates and excited to a sinusoidal transverse displacement. The samples were tested under uniaxial

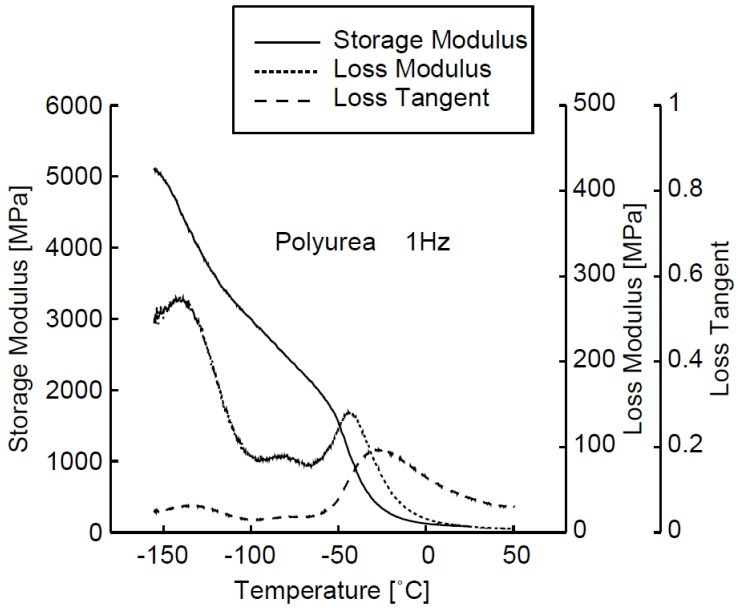

Figure 2.8: DMA Test Results of Polyurea Showing Storage Modulus, Loss Modulus, and Loss Tangent at a Frequency of 1 Hz Reproduced from Yi *et al.* (2006)

tension at a fixed frequency of 1 Hz and a strain amplitude of 0.1% from -156 to 80 °C was applied with a heating rate of 3 °C/min.

Average strain rate in DMA test was computed by the frequency dependence on the strain rate. The experiments were carried out over 1 Hz at a strain amplitude of 0.1%, corresponding to the strain rate of $2\text{x}10^{-3}$ respectively.

DMA results at a frequency of 1 Hz over the temperature range of -156 to -80 °C for storange modulus, loss modulus and loss tangent in its glass transition regime is plotted in Figure 2.8. Glass transitions were observed at -47° for polyurea, secondary transitions were observed at -80 °C, and more prominent gamma transition were observed at -141 °C. The mechanical behavior of the sample is known to be dependent on strain rate and the glass transition region of the storage is observed to shift with the strain rate in a linear manner. Thus the material mechanically recognizes the glass transition temperature at the given strain rate.

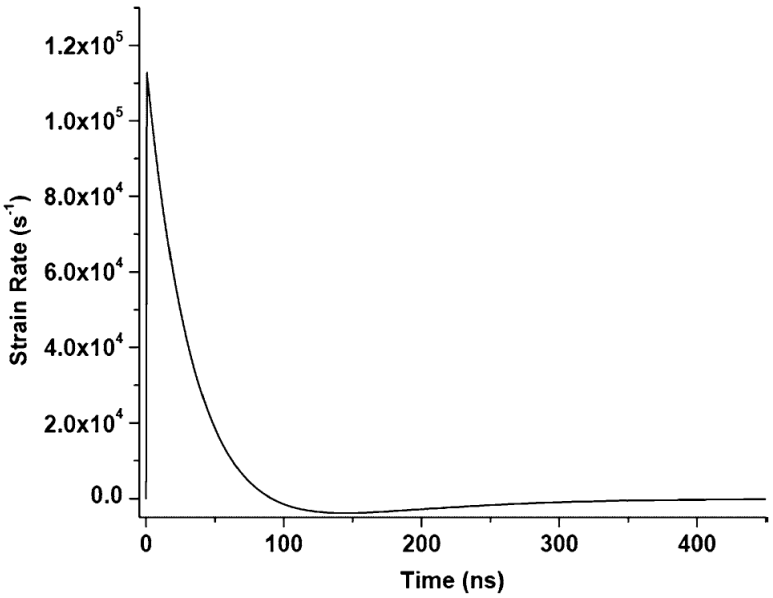

Figure 2.9: Strain Rate History of Polyurea During Deformation Reproduced from Youssef and Gupta (2012)

2.3.3 Ultrasonic Measurement

Polymer behavior at high strain rates was measured by Youssef and Gupta (2012) method using an apparatus and a test method which was based on laser-generated stress waves to obtain the material behavior.

Layers of thin polyurea becomes deformed by laser generated stress waves and experiences high strain rate of 1.1 x 10^5 s^{-1}. The total strain in the material remains less than 3%. Strain rate characteristics of the polyurea is shown in Figure 2.9. The strain rate experienced by the sample as a function of time is represented by Figure 2.9, which is not constant in the split-Hopkinson bar experiment during material deformation.

Thus different techniques and loading conditions are varied to obtain the strain rate and strain in the polyurea. Includes low to high strain rate and their correspond-

ing logarithmic strain of different methods for characterizing polyurea.

2.4 Failure Criteria

The response of polymers to the mechanical load is highly complex and stress plays a considerate role in the material failure. Since, evaluation of all the available stress combination tests cannot be provided, it is necessary to use a failure criterion generated on the general performance information about the material. Effects of the strain rate and temperature play an important role too, as they both have significant influence on the yield and failure of polymers. In this section failure criterion for polymers are explained in comparison with metals behaviour.

2.4.1 Void Formation and Growth

Shock waves are sharp discontinuities in pressure, density, and internal energy in a continuous material. They result from a localized, rapid release of energy, as in an explosion, or from high velocity impacts. The polymers under these shock waves were observed for the void formation.

A sample of the polyurea is (shown below in Figure 2.10) observed microscopically and after testing revealed the formation of voids of the order of 4-5 mm from the free-surface of the sample (Svingala *et al.* (2012)) and are easily observable. It is more likely that these voids are created by the interaction of release waves reflected from free-surfaces of the sample. A transient region of high tensile stress is produced by the interaction of these waves, leading to localized void nucleation (Chapman *et al.* (2005)). The formation and collapse of these voids leads to the more complex motion of the free-surface as a function of time.

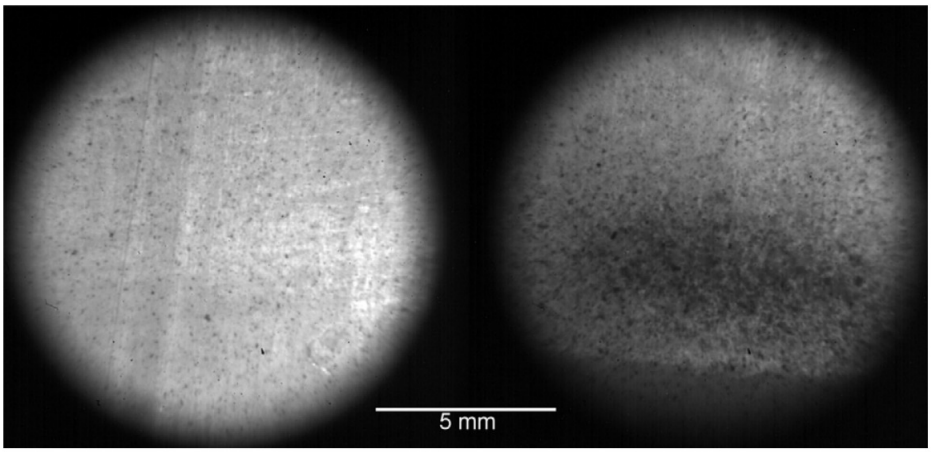

Figure 2.10: Untested Polyurea on the Left with Few Visible Voids and Voids Formed by the Shock Waves Reflects from the Surface of the Sample in Right Polyurea Reproduced from Svingala *et al.* (2012)

2.4.2 Yielding and Plasticity

According to a von Mises's theory, when the distortion energy density in a ductile material reaches a critical value it will yield. Where the critical value of the distortional energy can be estimated from the uniaxial test, as it is true for uniaxial stress state too.The distortional energy density is defined as,

$$U_d = \frac{1+v}{3E}{\sigma^2}_Y \tag{2.42}$$

This is the critical distortional energy density for the material, where σ_Y is the yield stress. Thus, according to von Mises's failure criterion, the material will yield when the distortional energy is equal or greater than the critical value for the material under multi-axial loading,

$$\frac{1+v}{3E}{\sigma^2}_{VM} \geq \frac{1+v}{3E}{\sigma^2}_Y \tag{2.43}$$

Similarly if we consider where only shear stress exists, such that stresses $\sigma_x = \sigma_y = 0$, and $\tau_{xy} = \tau$, and prinicpal stresses are $\sigma_1 = -\sigma_2 = \tau$ and $\sigma_3 = 0$. The line that will intersect the von Mises failure at two points is represented by the straight line at -45° which is a pure shear state on the σ_1 - σ_2 plane.

$$\sigma^2{}_Y = \sigma^2{}_1 + \sigma_1\sigma_2 + \sigma^2{}_1 = 3\sigma^2{}_1 = 3\tau^2{}_{max} \tag{2.44}$$

where,

$$\tau_{max} = \sigma_1 = \frac{\sigma_Y}{\sqrt{3}} = 0.577\sigma_Y \tag{2.45}$$

Thus, the material under shear stress yields when the shear stress reaches 0.577 of σ_Y.

Now, in case of the polyurea cavitation impact problem, von Mises yield criterion doesn't depend on the hydrostatic pressure which is temperature dependent due to the temperature dependence of elastic properties. However, sometimes cavitation without yielding is proposed as the cause of the failure (Asp *et al.* (1996)). It is instituted that von Mises failure criteria gives a conventional estimation of the yield-initiated failure whose intensity is evaluated as low in some regions and high in other regions. Thus it gives the conclusion of failure due to yielding in polyurea.

2.4.3 Maximum Principal Stress (Fracture)

According to the maximum principal stress theory, a brittle material fractures when the maximum principal stress in a material equals or exceeds the uniaxial tensile strength of the material. Modification of this theory for the ductile materials gives,

$$\sigma_1 \geq \sigma_v$$
$$\sigma_2 \geq \sigma_v \tag{2.46}$$

where σ_1 is the maximum principal stress and σ_v is the ultimate strength of the material.

The failure generated in the first and third quadrant coincides with the maximum shear stress theory which contained within the distortion energy theory. The envelopes in the second and fourth quadrants are well outside of the other two theories. Hence, the maximum principal stress theory is not considered satisfactory for ductile material.

In the case of polyurea principal stress theory, results are sensitive to temperature and loading rate. Most of the polyurea coating gives excellent durability and flexibility in cold temperatures. Nevertheless, there is a phase where in the beginning polyurea becomes brittle and cracks may occur leading to coating failure. Excessive movement of the flexible substrate may also result in coating fracture. Its concluded that the maximum principal stress theory can cause failure depending on the conditions linked with it. Sometimes stress may cause the little elongation up to 10% with two component epoxies having elongation combined with high tensile strength which represent excellent resistance however it also leads to fracture.

Chapter 3

NUMERICAL METHODS

Numerical modeling and finite element simulations were carried out to observe the material response to cavitation effects under impulsive pressure. Special attention is paid to observe the negative pressure and tensile stress in the material. In order to determine the behavior of the material, we will run finite element simulations and consider the influence of the following physical parameters: thickness of the coating, impact pressure magnitude, bubble size and load duration (Kim *et al.* (2014)).

3.1 Geometry

To examine the response of the material under the influence of various load parameters, multiple designed simulations are carried out.

The upper part of the domain is made up of polyurea, and the lower substrate part is composed of aluminum.

Domain size is based on the critical time step and is represented as (L_x, L_y). The impulsive pressure, which is generated due to bubble collapse, impacts the material, generating intense shock waves that result in cyclic stress loading, material wear, and deformation. Impulsive pressure is defined by the following equation (Kim *et al.* (2014));

$$P = P_{max} e^{-t/\tau - (x/R)^2} \tag{3.1}$$

P_{max} is the impulsive pressure generated at the wall by bubbles collapsing. In this investigation we consider P_{max} in the range of 0.5 - 3.0 GPa.

The radius of the bubble is determined by carrying out a few drastic simulations

(Amirkhizi *et al.* (2006)) and is defined over the range of 0.1 - 1 mm. Similarly, thickness of the polyurea coating varies thickness on the order of 0.1 - 2 mm.

When the bubble hits the surface, the rise time of the shock is set constant at 10ns. This is generally defined as 10 times the critical time step.

After the bubble collapses, the shock decays, and the time to decay is calculated by the characteristic time of the bubble dynamics,

$$\tau = R\sqrt{\rho/P_{collapse}}. \tag{3.2}$$

As represented by Eq. 3.2, the bubble collapse pressure is due to the driving pressure, which is a function of the ambient pressure driving the bubble collapse and is calculated by,

$$P_{max} = 3c\sqrt{\rho P_{collapse}}. \tag{3.3}$$

This gives,

$$P_{collapse} = \frac{P_{max}^2}{9c^2\rho_{H_2O}} \tag{3.4}$$

where density of the liquid (water) is constant, $\rho = 1000\text{kg/m}^3$.

Based on the above study, domain size is defined as,

$$L_{min} = \left(t_{fall} * \frac{C_{pu}}{2}\right) + R \tag{3.5}$$

$$H_{min} = \left(t_{fall} - \frac{t}{C_{pu}}\right) * \frac{C_{al}}{2} + t \tag{3.6}$$

where C_{pu} and C_{al} is the pressure wave speed in polyurea and aluminium, respectively.

3.2 Cavitation Load Profile

Loading on the material due to cavitation occurs. Collapsing bubble voids create heavy impulsive pressure (Choi *et al.* (2014)) and generate shock waves in the material. We carried out simulations to investigate the behavior of material. The top part of the domain is composed of thin polyurea with viscoelastic properties, and the bottom part is composed of a substrate of aluminium.

Loading on the material due to the cavitation effect was influenced by various load parameters, such as impact pressure, bubble radius, thickness of the material and the critical time step. These factors affected the material response and by changing these various variables, parametric simulations were carried out. In order to observe the polymer response, the collapse pressure was varied over 0.5 GPa to 3 GPa and material dynamics behavior was captured by keeping other parameters constant.

As soon as the materials are impacted by load they respond. The compressive stress waves reflect back due to material changes, though some waves still make it through the substrate. First, the compressive stress reaches the yield point and then complex deformations begin until the maximum load is reached.

Deformation due to the impact loads are also affected by the size of the collapsing bubble. Simulations indicates that the maximum deformation increases as the radial extent of the loading becomes larger. Characteristic radii are defined over the range of 10-1000 μm. The trend in deformation due to the radii extent of the load increases simultaneously as the radii extent increases. As the loading size increases the length of the domain increases simultaneously. We observed that length of the domain size should be at least twice the size of the bubble radii or else the stress waves will not have enough space to propagate and reflect back, leaving unusual residual stress on the polyurea.

It can be seen from the calculations that the decay time of shock keeps decreasing as the impact load pressure increases, which results in maximum deformation of the material. The trend remains the same for all thicknesses of the polyurea.

3.2.1 Axisymmetric

An axisymmetric condition is utilized to investigate the problem where the analysis of the domain is under axisymmetric loading. Axisymmetric, or radially symmetric, loading is easy to analyze as compared to other geometries or non-axisymmteric conditions.

Impact load due to cavitation is modeled axisymetrically. Various tests have been conducted for the evaluation of the stress, stress field, pressure and displacement of the system and the relationships between these factor under an axisymmetrically distributed loading on the plane surface of the film.

3.2.2 Integration Method

Explicit and implicit integration are two ways to carry out numerical analysis to obtain numerical solutions of time-dependent partial and ordinary differential equations. Explicit integration determines the state of system at a later time from the current state of the system, whereas implicit integration gives a solution by solving an equation involving both the current and later state of the system. The implicit method require an extra computation to solve the stiff equations at each time step, and thus required smaller steps to evaluate to keep the result error bounded. In this project, larger time steps are required, thus, the explicit integration method is implemented in finite element simulations runs.

3.2.3 Critical Time Step

Explicit integration plays an important role in non-linear dynamics. Under explicit codes, the central difference method is used when the time step is no larger than the critical time step. Generally, the critical time step is extremely small and the number of steps required for the simulation is large. Therefore, an accurate, reliable and efficient calculation is the most important.

It has been proven previously by some authors that the more the number of elements (N) in the finite element mesh, the larger the stability of the mesh will be (Amirkhizi *et al.* (2006)). Thus the critical time step is defined as the ratio of the size of the element to the pressure wave (p-wave) speed in the composite.

$$\Delta t = \frac{L}{C_{Al}} \tag{3.7}$$

where L is the length of the element size and C_{Al} is the speed in aluminium substrate.

$$C_{Al} = \sqrt{\frac{E}{\rho}} \tag{3.8}$$

The element based method (Flanagan and Belytschko (1984)) is the most efficient method in calculating the critical time step at every time step. However, this method produces a conservative estimate for the critical time step, and thus, for an efficient analysis the result from this critical time step method should be considered the upper limit.

Thus, the number of steps required for the finite element analysis is determined as,

$$NSteps = \frac{T}{\Delta t} \tag{3.9}$$

where T is the time required for simulation, and Δt is the critical time step as defined above in Eq 3.7.

The stability of the finite element wave propagation is dependent on the critical time step calculation. The central difference method for limiting the length of the time step in explicit integration is expressed as,

$$Cr_{crit} = \frac{2}{\omega} \tag{3.10}$$

where ω is a dimensionless frequency given by,

$$\omega = \frac{\omega_{max} H}{c_1} \tag{3.11}$$

where ω_{max} is the maximum natural frequency of a finite element mesh with H being element size and c_1 being speed of the wave propagation (longitudinal wave) in the continua.

3.3 Artificial Damping

Damping is the process of reducing, restricting and preventing the effect of oscillations. It describes how oscillations in the system decay. The idea of taking artificial damping into account is based on the addition of a damping term to the governing equations. It is useful to include realistic viscous damping as it brings stability to the numerical system.

3.3.1 Selecting the Damping Coefficients

Viscoelastic materials store some of the energy in a viscoelastic system and are recovered upon removal of the load, and the remainder is dissipated in the form of heat. The theoretical studies of the viscoelastic material state that dissipated energy

stored in the oscillation should be at least 100 times less than the kinetic energy in the material. The addition of passive damping can decrease peak vibration amplitudes in structural systems and add robustness to a marginally stable system (Ashley and Edberg (1986)). Also, the structural damping can be increased by several methods. The most common method for increasing the structural damping is the addition of high loss factor viscoelastic materials to the structure or the attachment of a mechanical vibration absorber (Hagood and von Flotow (1991)).

After careful analysis of viscoelastic measurements for damping in the material, we have selected a damping coefficient of $1x10^{-8}$.

3.3.2 Trade-off Between Conservation and Stress Oscillation

According to the principle of energy conservation, total energy in the system should remain constant (Kuhl and Crisfield (1999); Yim *et al.* (2003); Kuhl and Ramm (1996)). In our case, the total energy of the oscillating material is not constant. Thus, there must be a damping effect. The amount of energy dissipated is a measure of the structures damping level, which occurs progressively as energy is taken out of the system by another force. In physical systems, damping is produced by processes that dissipate the energy stored in the oscillation. Damping exists in all vibrating systems. It may be very small or very large depending on the system, and there is always a trade-off between conservation of energy and stress oscillation.

Run	P_{max} (GPa)	R (μm)	T_{rise} (ns)	T_{fall} (μs)
1	0.5	1000	10	9.0e-6
2	0.5	500	10	4.5e-6
3	0.5	10	10	9.0e-8
4	1.0	1000	10	4.5e-6
5	1.0	500	10	2.25e-6
6	1.0	10	10	4.5e-8
7	1.5	1000	10	3.0e-6
8	1.5	500	10	1.5e-6
9	1.5	10	10	3.0e-8
10	2.0	1000	10	2.25e-6
11	2.0	500	10	1.13e-6
12	2.0	10	10	2.25e-8
13	2.5	1000	10	1.8e-6
14	2.5	500	10	9.0e-7
15	2.5	10	10	1.8e-8
16	3.0	1000	10	1.5e-6
17	3.0	500	10	7.5e-7
18	3.0	10	10	1.5e-8

Table 3.1: Time to Pressure Fall Calculation

Chapter 4

RESULTS AND DISCUSSION

The finite numerical simulations of high impact pressure point loads on model polyurea are discussed. This chapter includes both the results as well as the conclusion derived from these results.

4.1 Effect of Temperature Rise in Polyurea

We conducted a series of simulations to numerically investigate the temperature rise in polyurea. The viscous energy dissipated from the polyurea is then calculated for different loading conditions.

The expected value of dissipated viscous energy from the polyurea under the impact of impulsive load is calculated. It shows, for the finite simulations, how much energy is dissipated from the polyurea by using the material model, as we discussed in Chapter 2.

Figure 4.2 shows curve fit when bubble radius and impact pressure magnitude varies simultaneously. Pressure is varied from 100MPa to 1GPa in an interval of 200MPa along with bubble radii varying from 100µm to 1mm in an interval of 200µm. The trend of total viscous energy dissipation from the polyurea is then observed.

For the number of repeated times the impacts occurring within the pressure and radii, gives expected dissipated viscous energy and can be defined as,

$$n(r,p) = \iint_0^\infty W_d(r,p)P(r,p)drdp \tag{4.1}$$

Thus, the viscous energy dissipated W_d as function of impact radius (r) and max pressure magnitude (p) from the FEM model is represented by,

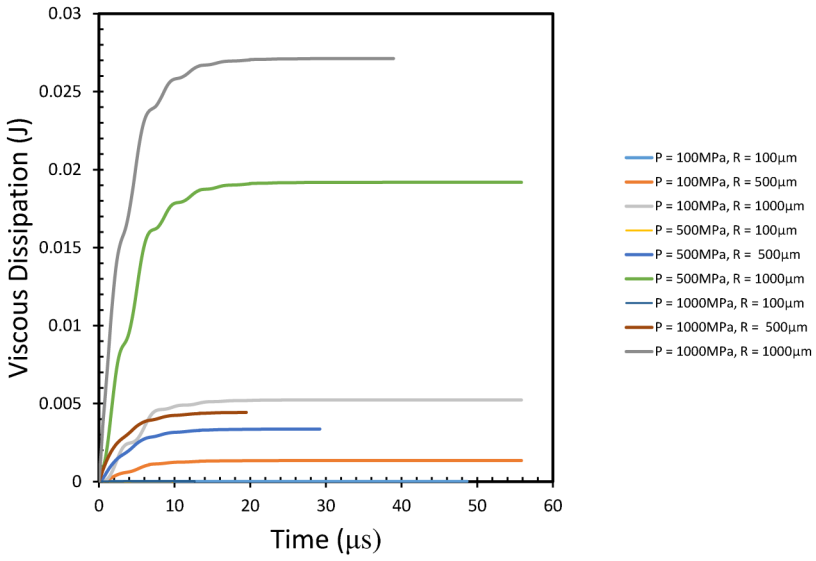

Figure 4.1: Viscous Dissipation from the Polyurea at Different Impact Magnitude and Bubble Radii

$$W_d = pr(c_0 p^2 r + c_1 p r^2 + c_2 r^2) \tag{4.2}$$

where, c_0, c_1, c_2 in Eq. 4.2 are fitted curve constants and their values are shown in Table 4.1

The above function represents the dissipated energy from the polyurea when it is subjected to different impact loads at different bubble collapse radii and can be used to evaluate the expected value of energy dissipation using two variable probability density functions as shown in Eq. 4.1.

The expected value from the two dimensional number of density distribution is calculated by the integral of the random variable with respect to probability measures which yields,

$$W_{ed} = 6NP^*(c_2 + 2P^*(c_1 + c_2 P^*/R^*)R^{*2}) \tag{4.3}$$

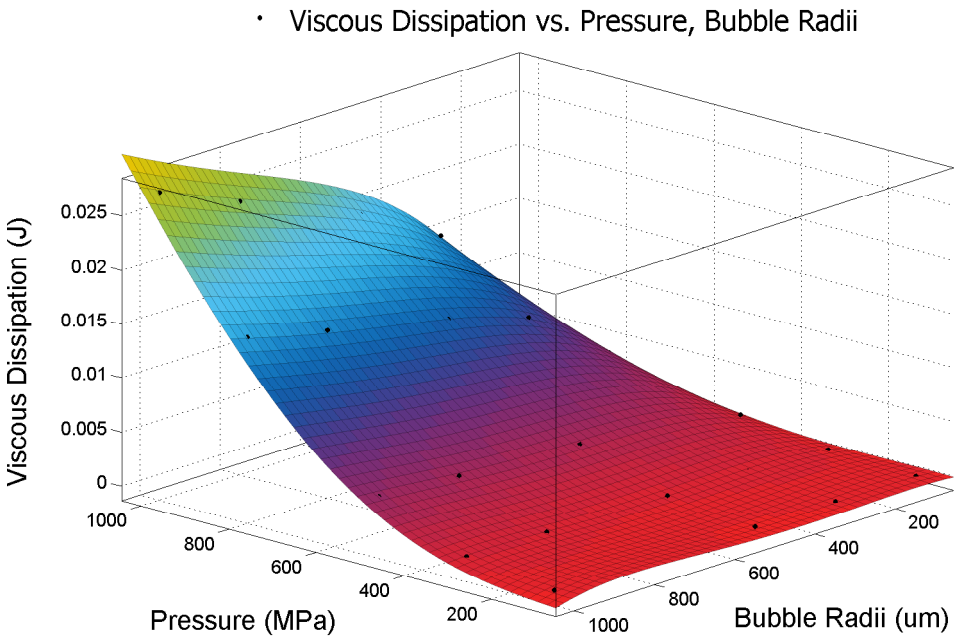

Figure 4.2: Fitted Curve Plot of Dissipated Viscous Energy from the Polyurea Sample

where, N is the number of impacts per unit area per unit time on polyurea layer. P^* is the characteristic amplitude of the impulsive pressure, and R^* is the characteristic bubble radii. Their values are calculated from (Kim *et al.* (2014)) as shown in table 4.1.

After solving for the Eq. 4.3, we arrive at the expected value of the dissipated energy as: 1.085 J/cm^2/sec which gives the temperature rise in material using following equations,

$$\Delta T = \frac{W_d}{Mass * C_p} \tag{4.4}$$

where, C_p is the specific heat capacity at constant volume and W_d is the dissipated viscous energy.

$$Mass = Volume * Density \tag{4.5}$$

therefore,

$$Mass = (\rho L^2 t) \tag{4.6}$$

Now, ΔT is evaluated as,

$$\Delta T = \frac{W_d L^2}{(\rho L^2 t) C_p} \tag{4.7}$$

$$\Delta T = \frac{W_d}{(\rho t) C_p} \tag{4.8}$$

Table 4.1: Parameters Used in Calculation

c_0:	2.195 x 10^{-28} J/Pa^3/m^2	N:	2416 impacts/cm^2/sec
c_1:	-5.119 x 10^{-16} J/Pa^2/m^3	P*:	4.01 x 10^8 Pa
c_2:	7.629 x 10^{-12} J/Pa/m^3	R*:	1.72 x 10^{-4} m
Density(ρ):	1.2 g/cm^3	Cp:	2.0 J/g/°C
Thickness(t):	1.0 mm		

Thus, the temperature rise in the polyurea with respect to time is 4.52 °C/sec.

Finally, in all simulations runs, maximum rise in temperature within polyurea is observed as 4.5 °C per unit time. This means that, it raise the significant temperature to cause failure in polyurea layer.

4.2 Parameter Study

Initially defined parameters are modified by carefully examining the outcomes of intense shock waves that propagate through the polyurea and substrate causing signif-

icant damage to the polyurea. The damage to the polyurea is due to the hydrostatic pressure observed in the polyurea region which is the indicative of failure.

After running a heavy work simulation, an intensive parameter study is carried out on the results. The combination of parameters that changes the behaviour of polyurea and damage it are then sorted.

Bubble size: Bubble generates in low pressure region and collapses within a liquid happens when the pressure in the liquid increases beyond a certain threshold. We observe this phenomena on the surface of polyurea, and from simulations, it is observed that primary size of bubbles that have the most impact are of the size 0.1 - 1mm.

Coating thickness: Polyurea coating behaviour under different levels of bubble size, impact pressure, rise time and domain is observed and is at carried out for varying thicknesses, from thickness of 0.2 - 1mm. The results at 0.1mm polyurea layer thickness gave significantly odd results. As the thickness kept on increasing the results become little significant. It is observed that, when we take sample with greater than 1mm thickness, the polyurea layer fails. It can't withstand high impact pressure.

Impact pressure: Bubble collapse pressure varies from 0.5 - 3.0 GPa but the limit after 2.0 GPa gives impractical results because the material becomes so deformed, that it can not be practically considered.

Outcomes Illustration: The flow of shock waves in the material consisting of polyurea and substrate are illustrated in the following section. Reflections, refractions of shock waves begin in the material which are discussed below.

4.2.1 Conclusions of Parameter Study

The conclusion of our research indicates that the when the thickness of the polyurea considered to be very less and the corresponding bubble radius very large,

then minimum negative pressure occurs after a number of reflections. Hence, the material observed will be safe from failure. In contrast, when the polyurea thickness considered is large, the pressure wave reaches interface and gives negative pressure instantly which cause failure. A pictorial representation follows the given explanation below.

4.3 Effect of Polyurea Coating Thickness

A parametric investigation is conducted to identify the effect of the polyurea coating thickness on the high pressure impacts mitigation. Various thicknesses of polyurea is observed subjected to impact loading. It has been found that the thin coatings of polyurea reduces the impact load effect, and prevents from failure. Three cases have been identified, which give substantial proof to the hypothesis that thinner coatings are stronger than thick coatings. Our conclusion is represented in the following paragraphs:-

Case1: When the thickness of the coating and bubble are considered to be the same, negative pressure is observed when the refraction wave hits interface which is just after when the bubble collapses at the surface and the wave propagates through the polyurea. In this case polyurea fails.

Case2: Simulated results shows that when the thickness of the polyurea is very large in comparison with the size of the bubble radius, the pressure wave propagates and minimum pressure occurs when the pressure wave reaches interface instantly, which leads to the polyurea failure. In this case, the polyurea layers fails to mitigate the impact load response, and the failure of layer observed.

Case3: When the bubble radius is considered to be larger than the thickness of the polyurea, the minimum pressure which is the tension in the material is observed after many reflections and cause failure to the material after so many reflection and

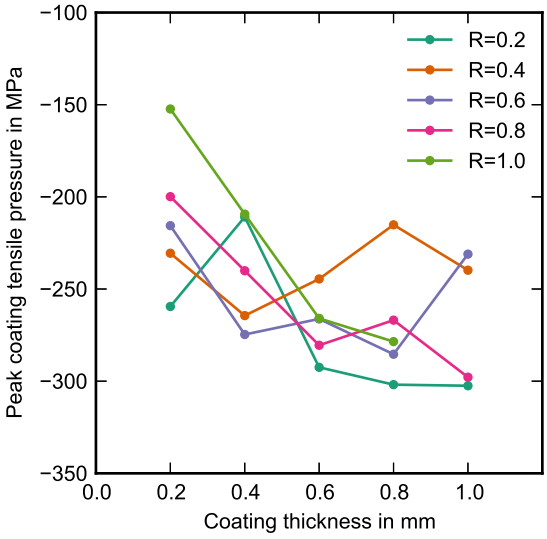

Figure 4.3: Peak Coating Tensile Pressure v/s Different Coating Thicknesses

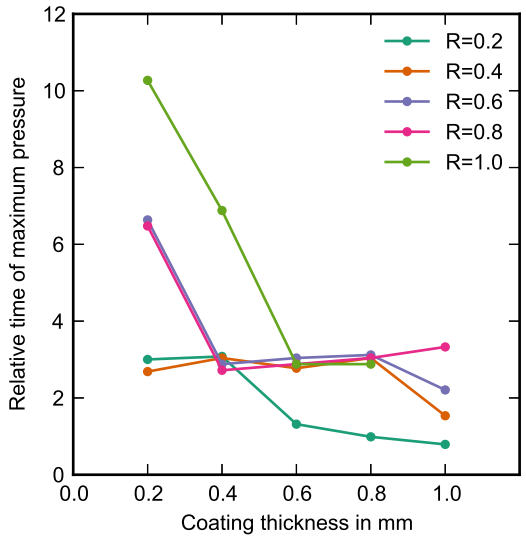

Figure 4.4: Relative Time of Maximum Pressure Rise in the Polyurea at Different Coating Thicknesses

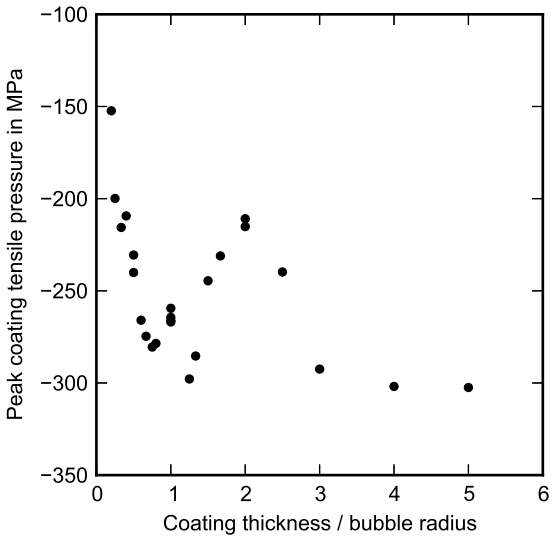

Figure 4.5: Peak Coating Tensile Pressure at Different Coating Thickness Relative to Bubble Radius

takes long period of time which is a good case. Thus, in this case, Polyurea survives the high pressure impact loading.

In Case 3, its clear that the thin layers of polyurea are stronger than the thick layers and can sustain high impact loads. Polyurea survives with no significant damage accumulation on the polyurea layer.

Chapter 5

CONCLUSIONS AND SUMMARY

This research investigated the response of polyurea coatings under high pressure impact load due to cavitation field. The complete temperature, pressure and strain-rate dependent viscoelastic constitutive model is used for the viscoelastic response of polyurea. Incorporated model accounts for the strain-rate effects as well as damage induced heating in the polyurea due to high pressure impacts. Parameters for constitutive models are extracted from the experiments. The prediction of the high pressure magnitude effect on the polyurea coating display reasonable agreement with the experimental observations.

5.1 Conclusions

The following responses are made regarding the high pressure impacts on the polyurea layer. The prediction of the final results indicates that the temperature have influence on the deformation of the polyurea and accumulate damage under varying loading conditions.

Parametric study also investigated that, thickness of the polyurea has a significant affect in the mitigation of failure due to high pressure cavitation field, where the thinner coatings lead to better protection.

5.2 Recommendations for Further Study

On the basis of above investigation on parameters, energy dissipation, and the temperature rise in the polyurea due to cavitation fields, leads to further analysis of the work which includes polyurea damage model evaluation.

Damage model may consist of evaluations of the pit analysis in the material which are the results caused by cavitation erosion. The large deformation, time dependent response of material under cyclic loading can be evaluated for a permanent set (Ayoub *et al.* (2014)). There have been numerous studies dealing with the cyclic loading on elastomers. A constitutive damage model can be developed to carry out the corresponding results at constant and variable amplitude loading conditions and can also be compared to the experimental data to see the alignment of the results.

REFERENCES

"Annual book of astm standards - section 3 material test methods and analytical procedures, vol. 03.02, american society for testing and materials (astm)", (2010).

Ahmed, S., K. Hokkirigawa, Y. Ito and R. Oba, "Scanning electron microscopy observation on the incubation period of vibratory cavitation erosion", Wear **142**, 2, 303–314 (1991).

Amirkhizi, A., J. Isaacs, J. McGee and S. Nemat-Nasser, "An experimentally-based viscoelastic constitutive model for polyurea, including pressure and temperature effects", Philosophical magazine **86**, 36, 5847–5866 (2006).

Ashley, H. and D. L. Edberg, "On the virtues and prospects for passive damping in large space structures", in "Proceeding of Damping", vol. 86 (1986).

Asp, L., L. Berglund and R. Talreja, "Prediction of matrix-initiated transverse failure in polymer composites", Composites Science and Technology **56**, 9, 1089–1097 (1996).

Ayoub, G., F. Zaïri, M. Naït-Abdelaziz, J.-M. Gloaguen and G. Kridli, "A visco-hyperelastic damage model for cyclic stress-softening, hysteresis and permanent set in rubber using the network alteration theory", International Journal of Plasticity **54**, 19–33 (2014).

Brennen, C. E., *Cavitation and bubble dynamics* (Cambridge University Press, 2013).

Brinson, H. F. and L. C. Brinson, *Polymer engineering science and viscoelasticity: an introduction* (Springer, 2007).

Carnelli, D., A. Karimi and J.-P. Franc, "Application of spherical nanoindentation to determine the pressure of cavitation impacts from pitting tests", Journal of Materials Research **27**, 01, 91–99 (2012).

Chapman, D., D. Radford, M. Reynolds and P. Church, "Shock induced void nucleation during taylor impact", International journal of fracture **134**, 1, 41–57 (2005).

Choi, J.-K., A. Jayaprakash and G. L. Chahine, "Scaling of cavitation erosion progression with cavitation intensity and cavitation source", Wear **278**, 53–61 (2012).

Choi, J.-K., A. Jayaprakash, A. Kapahi, C.-T. Hsiao and G. L. Chahine, "Relationship between space and time characteristics of cavitation impact pressures and resulting pits in materials", Journal of Materials Science **49**, 8, 3034–3051 (2014).

Flanagan, D. and T. Belytschko, "Eigenvalues and stable time steps for the uniform strain hexahedron and quadrilateral", Journal of Applied Mechanics **51**, 1, 35–40 (1984).

Foreman, J., S. Marcus and R. Blaine, "Thermal conductivity of polymers, glasses & ceramics by modulated dsc", SOC OF PLASTICS ENGINEERS, BROOKFIELD, CT,(USA). 1994. (1994).

Franc, J.-P. and J.-M. Michel, *Fundamentals of cavitation*, vol. 76 (Springer, 2006).

Franc, J.-P., M. Riondet, A. Karimi and G. L. Chahine, "Impact load measurements in an erosive cavitating flow", Journal of Fluids Engineering **133**, 12, 121301 (2011).

Hagood, N. W. and A. von Flotow, "Damping of structural vibrations with piezoelectric materials and passive electrical networks", Journal of Sound and Vibration **146**, 2, 243–268 (1991).

Kim, K.-H., G. Chahine, J.-P. Franc and A. Karimi, *Advanced Experimental and Numerical Techniques for Cavitation Erosion Prediction* (Springer, 2014).

Knauss, W., "Viscoelastic material characterization relative to constitutive and failure response of an elastomer", Tech. rep., DTIC Document (2004).

Kuhl, D. and M. Crisfield, "Energy-conserving and decaying algorithms in non-linear structural dynamics", International journal for numerical methods in engineering **45**, 5, 569–599 (1999).

Kuhl, D. and E. Ramm, "Constraint energy momentum algorithm and its application to non-linear dynamics of shells", Computer Methods in Applied Mechanics and Engineering **136**, 3, 293–315 (1996).

March, P., "Evaluating the relative resistance of materials to cavitation erosion: a comparison of cavitating jet results and vibratory results", in "ASME cavitation and multiphase flow forum, Cincinnati", pp. 14–17 (1987).

Murata, H., "Rheology–theory and application to biomaterials", Edited by Ailton De Souza Gomes p. 403 (2012).

Nemat-Nasser, S., J. B. Isaacs and J. E. Starrett, "Hopkinson techniques for dynamic recovery experiments", Proceedings of the Royal Society of London. Series A: Mathematical and Physical Sciences **435**, 1894, 371–391 (1991).

Pereira, F., F. Avellan and P. Dupont, "Prediction of cavitation erosion: an energy approach", Journal of Fluids Engineering **120**, 4, 719–727 (1998).

Qiao, J., A. V. Amirkhizi, K. Schaaf, S. Nemat-Nasser and G. Wu, "Dynamic mechanical and ultrasonic properties of polyurea", Mechanics of Materials **43**, 10, 598–607 (2011).

Soyama, H., A. Lichtarowicz, T. Momma and E. J. Williams, "A new calibration method for dynamically loaded transducers and its application to cavitation impact measurement", Journal of fluids engineering **120**, 4, 712–718 (1998).

Svingala, F., M. Hargather and G. Settles, "Optical techniques for measuring the shock hugoniot using ballistic projectile and high-explosive shock initiation", International Journal of Impact Engineering **50**, 76–82 (2012).

Tekalur, S. A., A. Shukla and K. Shivakumar, "Blast resistance of polyurea based layered composite materials", Composite Structures **84**, 3, 271–281 (2008).

Thamsen, P., T. Bubelach, T. Pensler and P. Springer, "Cavitation in single-vane sewage pumps", International Journal of Rotating Machinery **2008** (2008).

Thiruvengadam, A., "Handbook of cavitation erosion.", Tech. rep., DTIC Document (1974).

Yi, J., M. Boyce, G. Lee and E. Balizer, "Large deformation rate-dependent stress–strain behavior of polyurea and polyurethanes", Polymer **47**, 1, 319–329 (2006).

Yim, J. H., S. Y. Cho, Y. J. Seo and B. Z. Jang, "A study on material damping of 0 laminated composite sandwich cantilever beams with a viscoelastic layer", Composite structures **60**, 4, 367–374 (2003).

Youssef, G. and V. Gupta, "Dynamic response of polyurea subjected to nanosecond rise-time stress waves", Mechanics of Time-Dependent Materials **16**, 3, 317–328 (2012).

Zhang, S., J. H. Duncan and G. L. Chahine, "The final stage of the collapse of a cavitation bubble near a rigid wall", Journal of Fluid Mechanics **257**, 147–181 (1993).